

Supporting Information

Quantitative Analysis of Amyloid Polymorphism Using Height Histogram to Correct for Tip Convolution Effects in Atomic Force Microscopy Imaging

Yi-Chih Lin¹, Hiroaki Komatsu², Jianqiang Ma³, Paul H. Axelsen², and Zahra Fakhraai¹

A. Height Histogram Simulation from Ideal Cross-Section to AFM Measurement

The mica fit in Figure 1D defines the systematic noise in AFM measurement. This information can be used to simulate the height histogram of AFM measurement from ideal cross-section of TMV. We assume the height point in the cross-section profile (Figure 2B) has the same height variation as mica's Gaussian fit (systematic noise) in the experimental measurement. The pre-fitted, normalized Gaussian function is shown below.

$$f = e^{-0.5 \times \frac{(h-h_0)^2}{0.092^2}}, \text{ where } h_0 \text{ is the height value of the data point being broadened}$$

Therefore, each bar in the ideal height histogram (red bar in Figure 2C) becomes broadened as shown in Figure 2C. In Figure S2, the strong agreement between AFM experimental data and simulated result indicates the evolution of height from ideal situation to real AFM data can be simulated by just considering the substrate roughness and the uncertainty of the AFM measurement in defining the height of a nanostructure. The shift of TMV peak is mainly attributed to the difference between measured maximum height in experiment (~16.8 nm) and ideal maximum height assumed in theory (17.0 nm).

B. Structural Characterization of Polymorphs in Large-Area Image

Based on the characteristic height profiles of various polymorphs, as identified in single fibril section, six types of polymorphs can be recognized in Figure 5A, highlighted in a larger version of this image in Figure S4. The height profiles of these fibrils are similar to the single fibril results, but fewer number of points are measured per fibril due to the decreased image resolution. Also, some structural features (*e.g.* pitch distance and fibril width) are not resolved in this image.

C. Simulated Enlargement of the Measured Width (ΔW) for a Cylindrical Nanostructure

Based on our proposed model (Figure 2A), the object's height, its geometry, and tip sharpness will influence the degree of tip-dilation. The tip coating and tip material only change the intrinsic properties, *e.g.* the resonance frequency, hardness, conductivity, which is not considered in our model under the assumptions of no tip-induced compression and tip-object interactions. Figure S7A displays our model to evaluate the enlargement (ΔW) caused by tip-dilation. When tip radius (b) is larger than object's radius (a), the measured width ($2W$) is equal

to $\sqrt{8bH}$ ($H = 2a$, object's height). Once $b < a$, the tip's geometry near apex controls the tip-object contact. Assuming the tip's geometry is almost vertical, the measured width becomes equal to $H + 2b$. The ΔW can be further defined as the difference between the measured width ($2W$) and the object's width ($2a$). In Figure S7B, the object's height (H) is plotted versus enlargement (ΔW) for the AFM tip used in this study ($b = 10 \text{ nm}$). This figure shows that the ΔW reaches a plateau when $H > 20 \text{ nm}$ for a cylindrical objects. Figures S7C and S7D show the influence of tip sharpness on the ΔW of TMV particle ($a = 8.5 \text{ nm}$) and cylindrical fibrils ($a = 2 \text{ nm}$). We note that even though the amyloid fibrils are not simply cylindrical in shape, the geometrical factor doesn't change the ΔW due to the nature of the tip dilation which only affect the data on the two edges of an object. The object's geometry can be further modified as elliptical cylinder or other geometries, which merits further studies and will be addressed in the future.

D. Evaluation of Amyloid Polymorphism under different Experimental Conditions

The histogram analysis can provide the relative volume percent (V%) of each amyloid polymorph displayed in an AFM image. To evaluate the variation of V%, we measured the amyloid sample under different experimental conditions.

Scan speed: The scan speed in all experiments (including the data shown below) is set as 0.4-0.6 line per second for high quality images. Admittedly, higher scan rates can result in lower resolution images affecting all data accordingly. However, in this paper, we assume that given all other limitations quasi-static scan rates can be used for imaging.

Image resolution: Figure S8 shows the influence of scan resolution on the height histogram analysis. When the same scanner is used (multi-purpose XYZ closed-loop scanner equipped with 10 nm AFM tip used in the manuscript), the increase of scanning resolution (pixel/line) slightly broadens the feature peak near 4 nm in Figure S8C, but does not significantly change the shape of height histogram. Therefore, the relative V% of each amyloid polymorph will be similar in both AFM images. In general, image resolution only helps improve the statistics by providing larger number of data points for rare population (on the lower side of the most probable heights), but images still suffer from the tip convolution problem.

Tip Sharpness: Figure S9 shows the effects of tip-sharpness while using a high-resolution scanner (9 μm in XY and 2 μm in Z direction). The combination of high-resolution scanner and ultra-sharp tip can clearly provide more distinct peaks in the height histogram (Figure S9C) by suppressing the tip-dilation effect. Figure S9D shows the calculated V% of each polymorph displayed in Figure S9A and S9B and compares the result with the data reported in the manuscript. Compared to the FIT 2 listed in the manuscript, the results of high-resolution images shown in Figure S9 have some variation in the V%. However, most of this variation can be attributed to (1) the differences in the content when the scan area is changed, in particular for less abundant species, and (2) the small scan size for these images (9 μm^2) compared to the one provided in the main paper (25 μm^2). To provide a more reliable v%, one can follow up our

suggestions in the manuscript to increase the sample size. This data shows the robustness of this method in quantifying the mass content of various polymorphs, but also the potential sources of error.

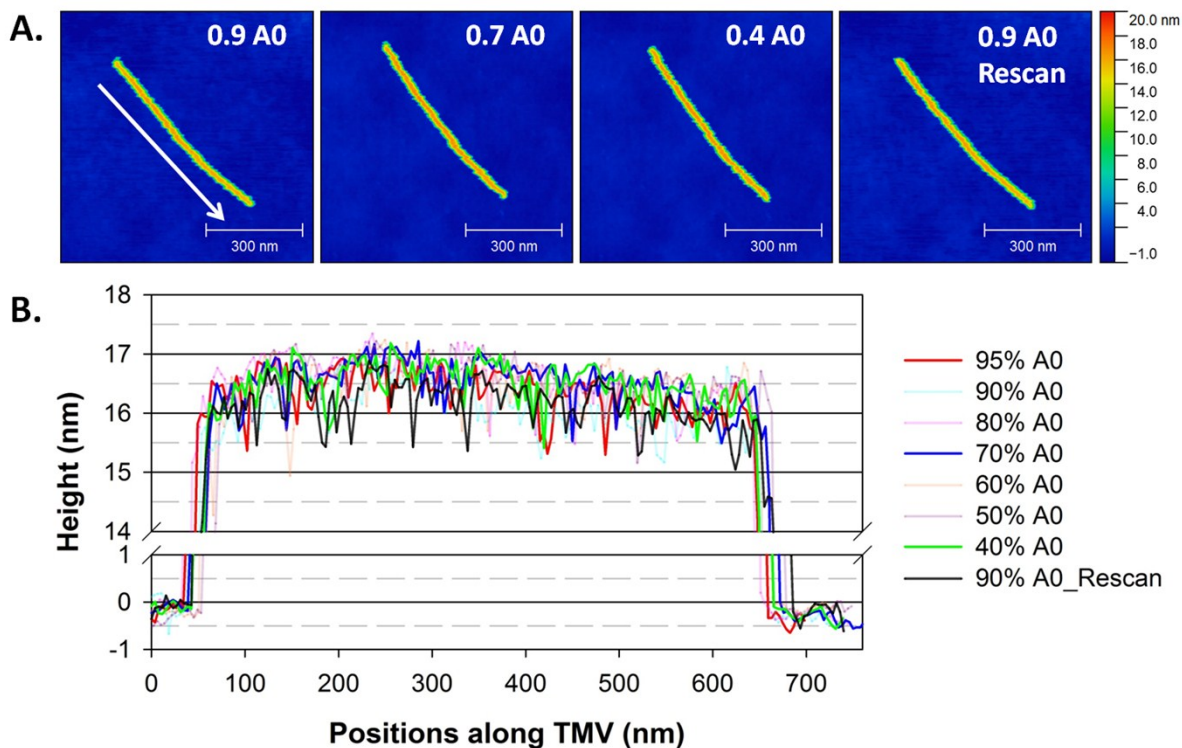


Figure S1. Continuous TMV measurements in tapping mode under various set points for the oscillation amplitude. (A) A TMV particle, deposited on silicon wafer, was imaged from 90% to 40% of the free oscillation amplitude (A0), and then rescanned at 90% of A0. (B) The height profiles of the imaged TMV along the direction of white arrow indicated in A. The decrease of setting oscillation amplitude results in the increase of applied force on TMV during AFM measurement. There is no significant height compression or tip-induced destruction in our tapping AFM measurements.

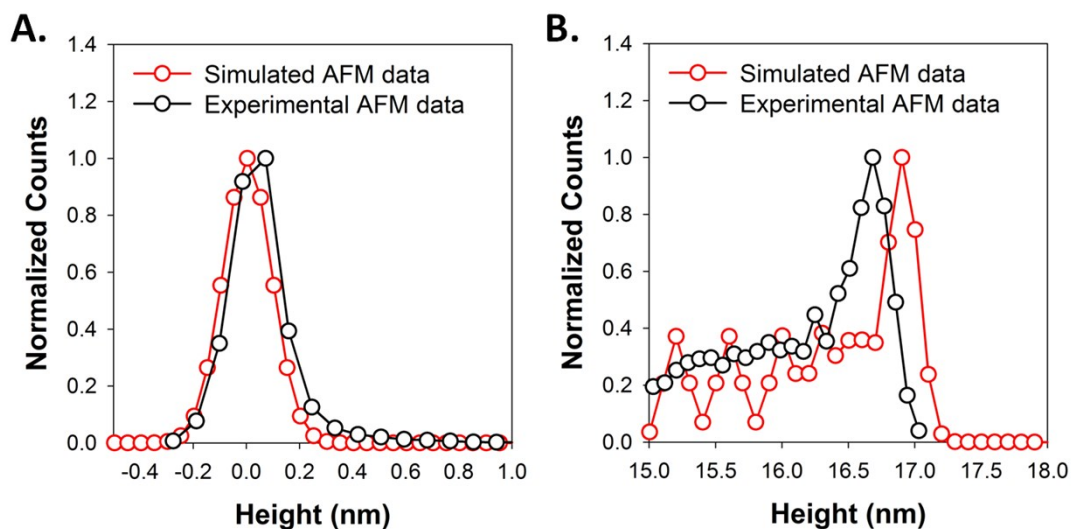


Figure S2. The comparison between simulated and experimental AFM height histogram of a TMV particle. (A) The mica substrate peak for simulated data (red) and the experimental AFM data (black). Both peaks match well. (B) The normalized height distributions from 15.0 nm to 18.0 nm. The similar shape and height position of both peaks indicate the simulation can well describe the evolution from an ideal cross-section to real AFM measurement. The peak shifting is mainly attributed to the difference between ideal maximum height in assumed for simulations (17.0 nm) and measured maximum height in experiment (~ 16.8 nm).

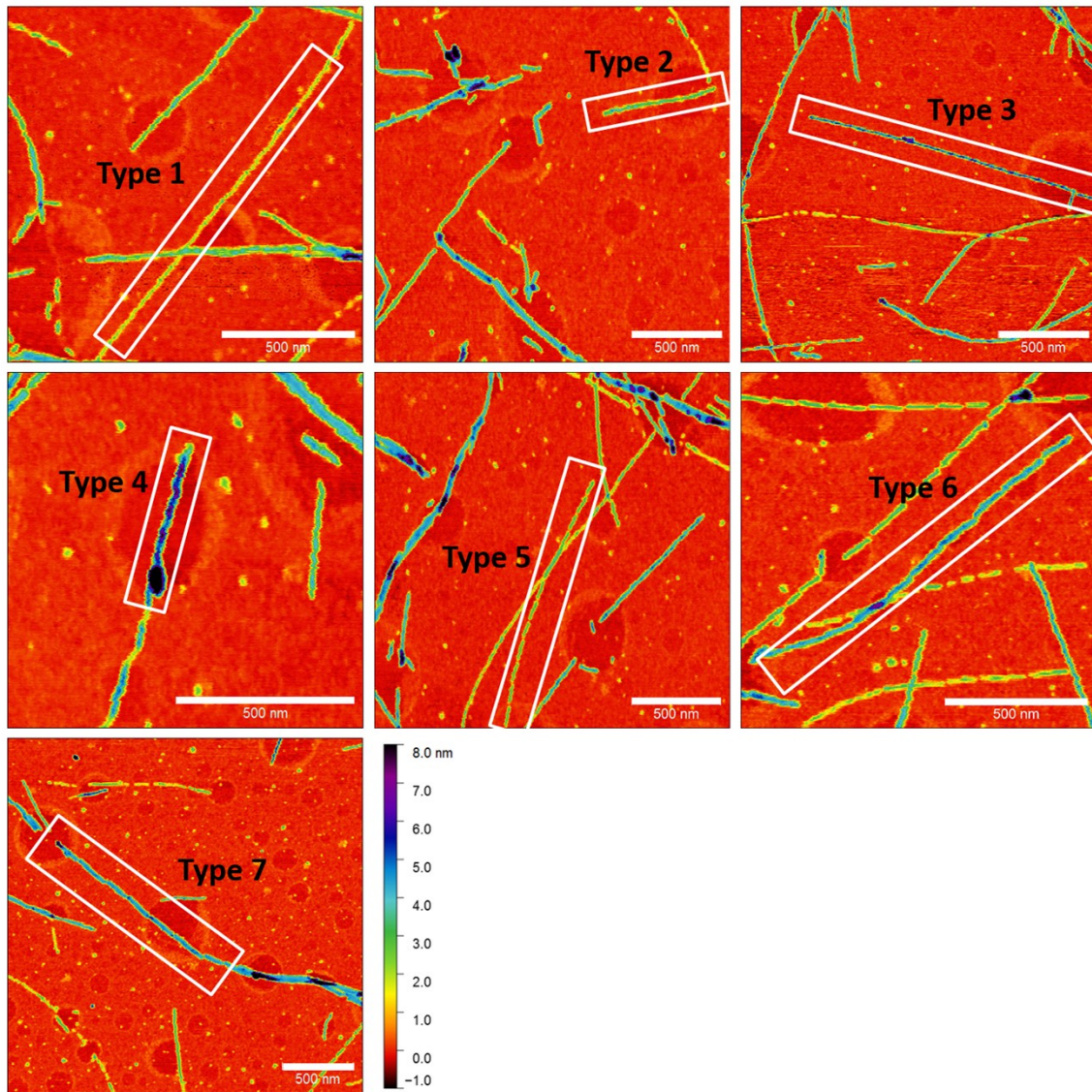


Figure S3. Original AFM images (512×512 pixels) of different fibrils used for single fibril analysis in Figure 4.

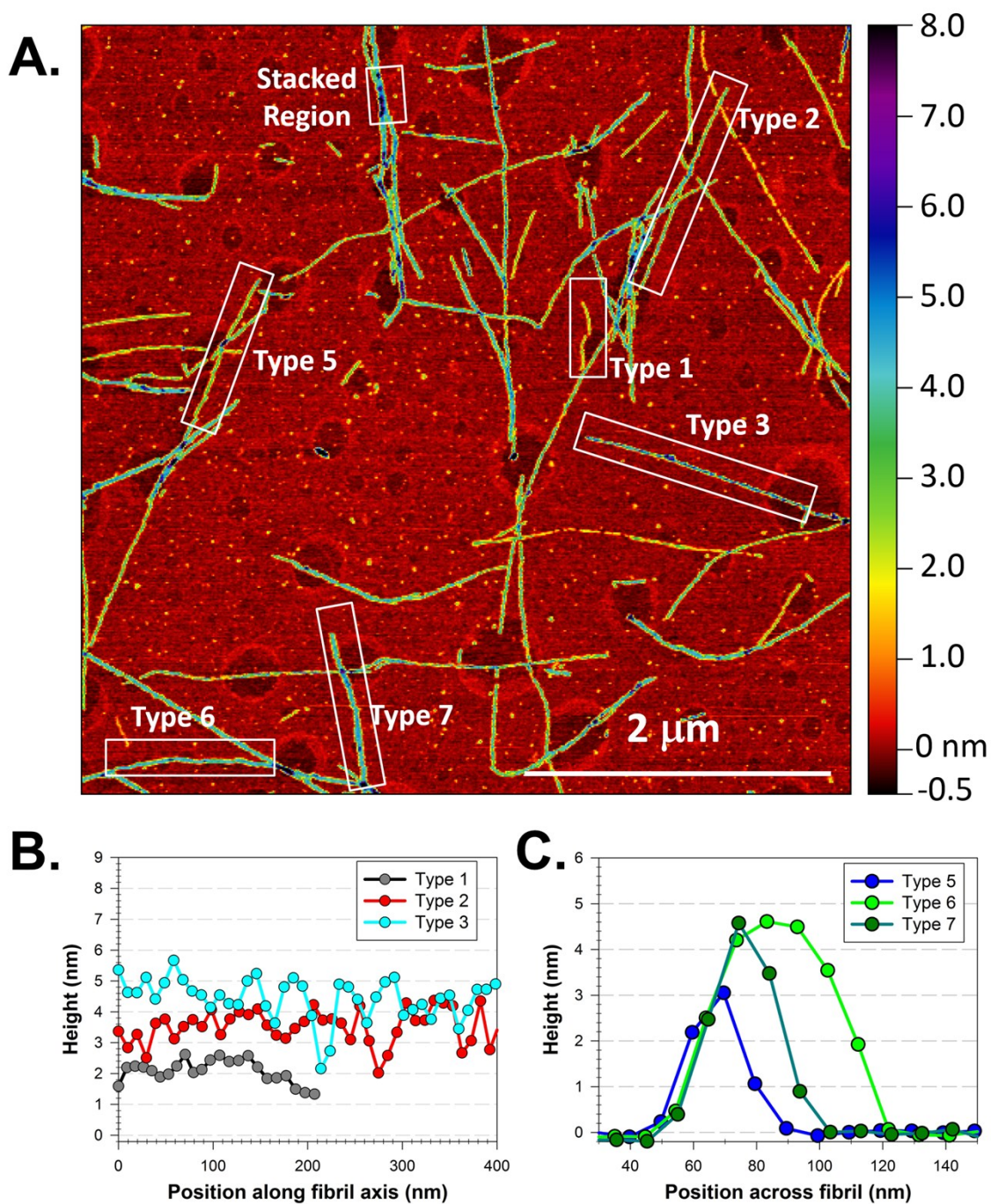


Figure S4. (A) Large area AFM image showing the polymorphism of $A\beta_{40}$ fibrils (Figure 5A). The featured fibrils are labeled according to the characterization described in the manuscript. Type 4 fibril is not observed in this image. (B and C) The height profiles of various type structures (B) along the twisted fibril's axis and (C) across the striated-ribbon like fibril, marked in the top image by white boxes. For each type of fibril, the height variations on the fibril's backbone are similar to the single fibril results. However, some detailed features are not clearly visible due to the lower relative image resolution for a large area image compared to single fibril data.

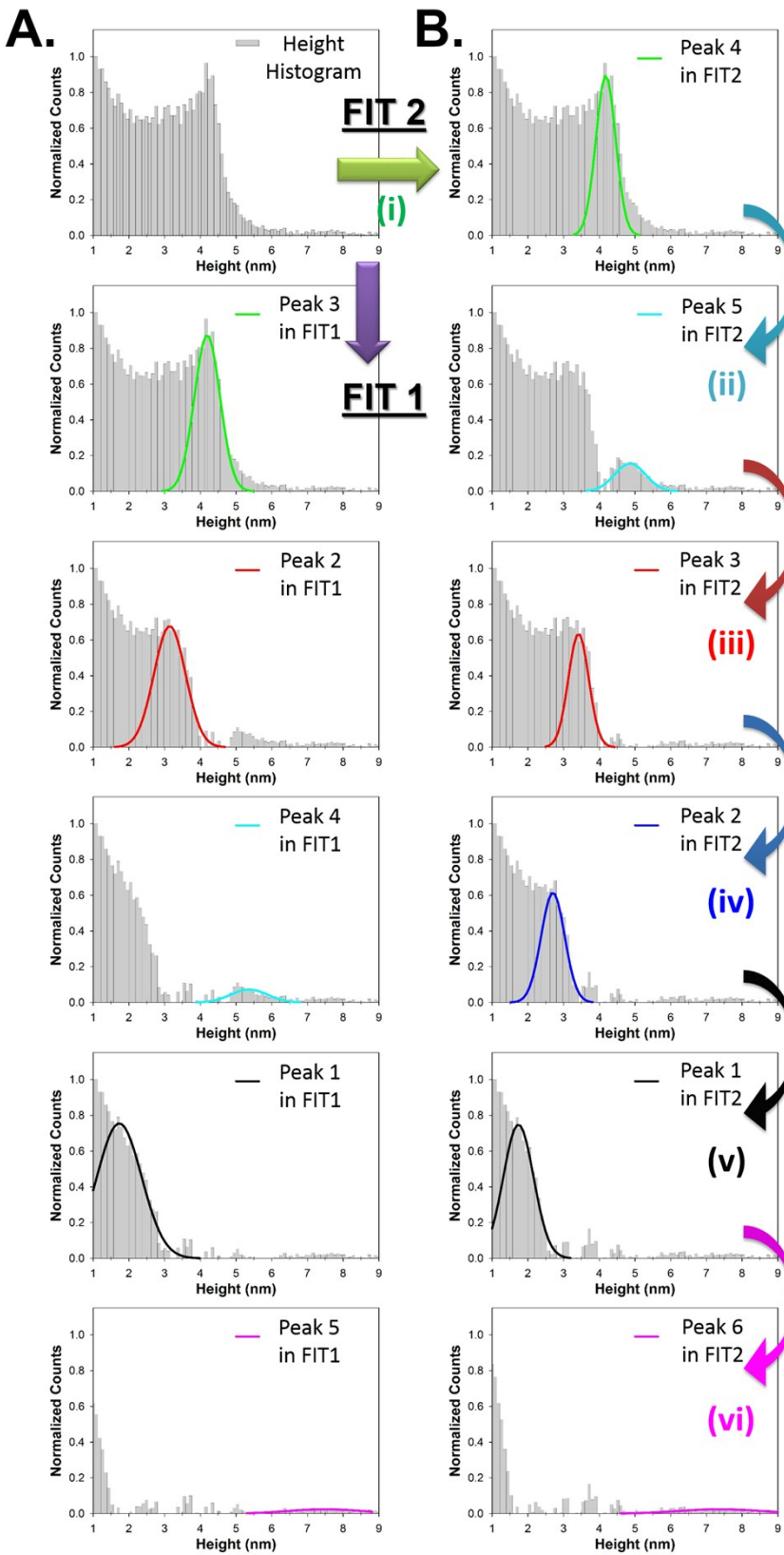


Figure S5. Step-wise fitting procedures for the height histogram plot of large area AFM image in Figure 5A. FIT 1 is a free-fit without any limitation on the peak positions or peak widths. FIT 2 is utilizing the height information from single fibril analysis (Table 1) as initial fitting parameters to deconvolute the height histogram curve. The initial fitting parameters for peak center and peak width are originated from (i) Type 6 (4.2 ± 0.3 nm), (ii) Type 3 (5.0 ± 0.5 nm), (iii) Type 2 (3.3 ± 0.6 nm), (iv) Type 5 (2.9 ± 0.2 nm), (v) Type 1 (1.9 ± 0.4 nm), and (vi) Type 4 fibril (7.4 ± 0.4 nm). We note that only the peak width (± 0.3 nm) in (i) is fixed during fitting. The reason for applying six fits in FIT2 is that the featured heights of Type 6 and Type 7 are very similar. They can be considered as sharing the same characteristic heights, 4.2 ± 0.3 nm in step (i). The results are summarized in Table 2.

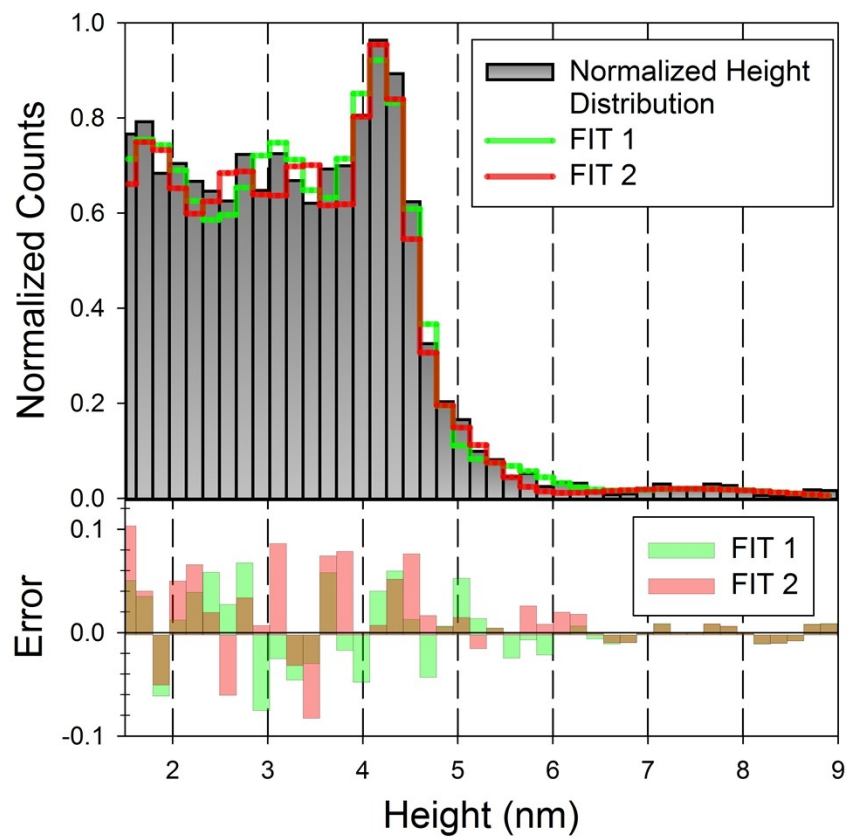


Figure S6. A comparison between constrained and unconstrained fitting procedures in Figure 5. *Top:* The FIT 1 (green) and FIT 2 (red) are the sum of fitted Gaussian functions used to fit data in Figure 5. *Bottom:* The error plot is the difference between original height histogram and the curves shown in the top figure, generated by the sum of Gaussian functions.

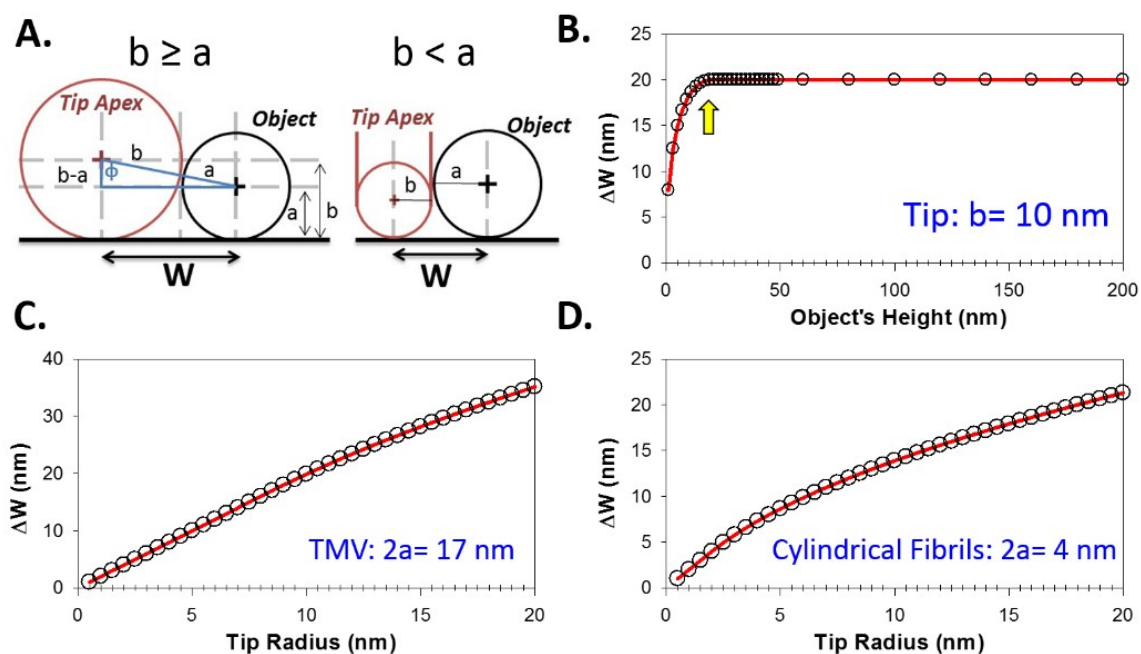


Figure S7. The simulated enlargement of the measured width (ΔW) for a cylindrical nanostructure due to the tip-dilation effect. (A) The relative geometry between the tip (b nm in radius) and cylindrical object (a nm in radius). The enlargement (ΔW) is defined as the difference between object's width ($2a$) and the measured width ($2W$). (B) The influence of object's height (H) on the ΔW using 10 nm AFM tip (expected tip radius used in experiments). The yellow arrow indicates that the enlargement becomes fixed when the tip and object are in the same size ($H = 2a = 2b$). (C, D) The influence of tip sharpness on the ΔW for TMV and cylindrical fibrils, respectively.

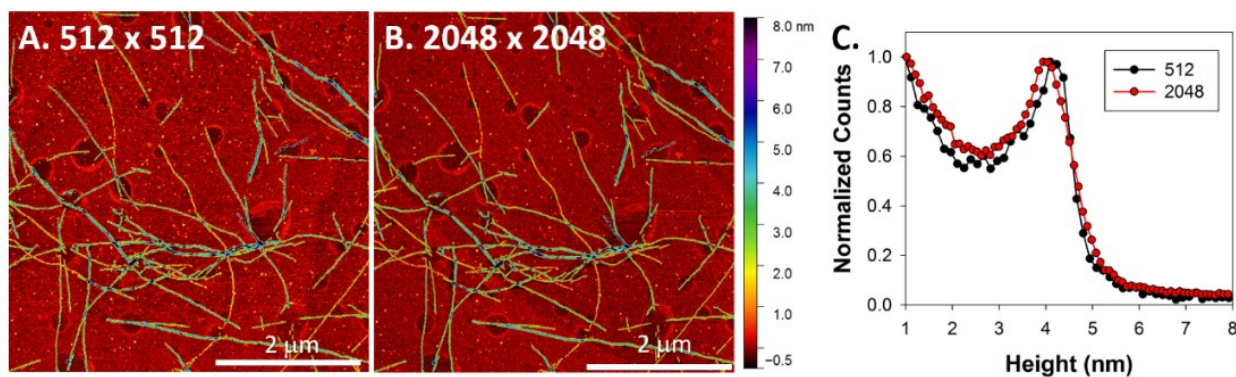
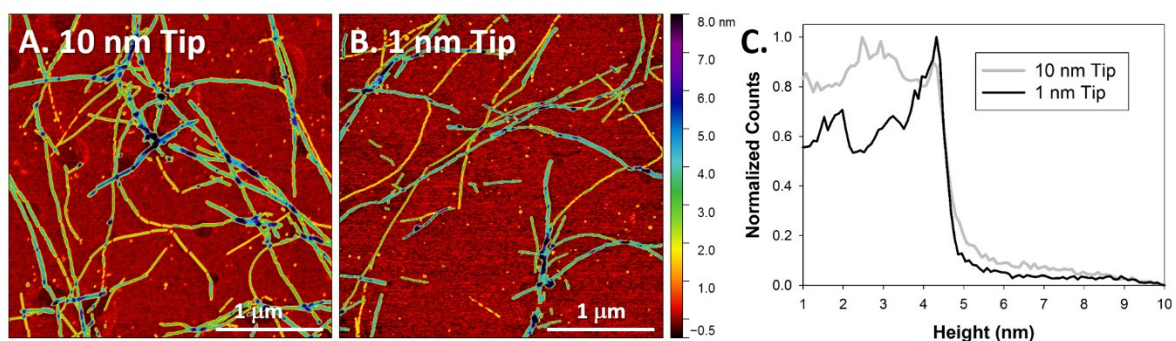


Figure S8. The effect of scanning resolution (pixel/line) on the height histogram of an AFM image that contains multiple polymorphs. (A, B) Large-area AFM images using different pixel/line values. (C) The normalized height histograms for the AFM images with different pixel/line values. In this set of experiments, the multi-purpose XYZ closed-loop scanner was used along with the same tip used in the manuscript (Tap-300AIG, Budget Sensors).



D. “FIT2 in manuscript” “A” (10 nm tip with HR-scanner) “B” (1 nm tip with HR-scanner)

	$H_{\text{mean},S}$	V%	Assignment	$H_{\text{mean},S}$	V%	$H_{\text{mean},S}$	V%
Peak 1	1.8 ± 0.4	27.9 %	PFs Type 1	1.5 ± 0.4	23.3 %	1.7 ± 0.4	27.3 %
Peak 2	2.7 ± 0.3	19.7 %	Type 5	2.5 ± 0.4	24.3 %	2.7 ± 0.4	18.6 %
Peak 3	3.5 ± 0.3	17.6 %	Type 2	3.3 ± 0.4	24.4 %	3.5 ± 0.4	20.2 %
Peak 4	4.2 ± 0.3	24.0 %	Type 6 Type 7	4.3 ± 0.3	18.7 %	4.3 ± 0.3	28.4 %
Peak 5	4.9 ± 0.4	6.5 %	Type 3 Type 4	5.1 ± 0.3	3.2 %	5.1 ± 0.3	3.0 %
Peak 6	7.4 ± 1.2	2.5 %	Type 4 Region with overlaps	6.5 ± 1.3	6.1 %	7.2 ± 1.8	3.5 %

Figure S9. The influence of tip-sharpness on the height histogram of an AFM image that contains multiple polymorphs. (A, B) Large-area AFM images scanned by 10 nm AFM tips (Tap-300AlG, Budget Sensors) and 1 nm AFM tip (SHR150, Budget Sensors), respectively. The image resolution is 512×512 pixels for both images. We note that the used AFM scanner was a high-resolution scanner (9 μm in XY and 2 μm in Z direction) and different than the one used in the main paper. (C) The normalized height histograms for both AFM images. (D) The comparison of volume analysis between FIT 2 (demonstrated in the manuscript) and the AFM images measured by HR-scanner equipped with tips with different sharpness.

Table S1. The results of TMV height analysis

AFM Tip: 300 KHz (k=40 N/m)

$H_{max,P}^a$: 16.81 ± 0.08 (n=20)

$H_{mean,S}^b$: 16.65 ± 0.17

All units are in nm. ^a The average of maximum heights ($H_{max,P}$) are analyzed from the imaging profiles in Figure 1A, using the profile tool in Gwyddion software. The uncertainty is the standard deviation of the measured maximum heights. n is the number of studied samples. ^b The statistical mean height ($H_{mean,S}$) is calculated as the difference between two Gaussian peaks in the height histogram (Figure 1D), one for the mica substrate and another for TMVs. The uncertainty is one standard deviation of TMV's Gaussian fit (σ_{TMV}).